Measurement of ^{59}Co(n, x) reaction cross sections with the fast neutrons based on the ^{9}Be(p, n) reaction*

Muhammad Zaman[1] Muhammad Nadeem[1] Muhammad Sahid[1] Kwangsoo Kim[1]
Guinyun Kim[1†] Nguyen Thi Hien[1,2]

[1]Department of Physics and Center for High Energy Physics, Kyungpook National University, Daegu 41566, Republic of Korea
[2]Institute of Physics, Vietnam Academy of Science and Technology, 10 Dao Tan, Hanoi, Vietnam

Abstract: The cross sections of the ^{59}Co(n, x) reaction in the average energy range of 15.2-37.2 MeV were measured using activation and an off-line γ-ray spectrometric technique. The neutrons were generated from the ^{9}Be(p, n) reaction with proton beam energies of 25-45 MeV at the MC-50 Cyclotron facility of the Korean Institute of Radiological and Medical Sciences (KIRAMS). Theoretical calculations of neutron–induced reactions on ^{59}Co were performed using the nuclear model code TALYS-1.9. The results for the ^{59}Co(n, x) reactions were compared with the theoretical values obtained using TALYS-1.9 and the literature data provided in EXFOR and the TENDL 2019 nuclear data library. The theoretical values obtained using TALYS-1.9 with adjusted parameters are comparable to the experimental data. The measured reaction cross sections of a few radionuclides are new, and the others are comparable to the literature data, and thus, they can strengthen the database. The present study on cross sections leads to useful insight into the mechanisms of ^{59}Co(n, x) reactions.

Keywords: ^{59}Co(n, x) reaction cross sections, average neutron energy of 15.2-37.2 MeV, off-line γ-ray spectrometry, MCNPX 2.6.0 simulation, TALYS-1.9

DOI: 10.1088/1674-1137/abe196

I. INTRODUCTION

Neutron-induced reaction cross sections play a major role in the current nuclear science regarding human life. Such microscopic data are necessary for practical and theoretical applications. Evidently, with an increasing number of nuclear data applications, the requirements of nuclear data are also increasing [1]. Accurate knowledge of the cross section for neutron-induced reactions on ^{59}Co is of importance owing to its use as a structural material in fission and fusion reactors as well as its applicability to neutron dosimetry [2]. The natural cobalt element (^{59}Co) can be used as a target material for the production of medically and technologically important ^{56}Co, ^{57}Co, ^{58}Co, ^{54}Mn, and ^{59}Fe radionuclides. Among these, ^{55,57,58}Co offer potential applications in the synthesis of radio pharmaceuticals, research, and radiotherapy owing to their suitable decay characteristics. Moreover, ^{54}Mn is used for calibrating γ-ray detectors, labeling and tracing the transport of manganese containing materials, and treating hematologic diseases owing to the emission of low energy electrons. As a mono-energetic γ-ray emitter, it also reveals the shape parameters of a detector spectrum, such as the peak-to-total ratio. As natural cobalt is a mono-isotopic (^{59}Co) element, its neutron-induced reaction cross sections are suitable for the verification, testing, and improvement of theoretical models [3, 4]. Furthermore, the theoretical prediction of nuclear cross-section data is crucial in the absence of experimental data [5].

The nuclear reaction cross sections induced by different energy neutrons and photons remains a major problem in applications such as data evaluation [6], applied nuclear physics, nuclear models, and nuclear reaction codes [7]. Therefore, an experimental study on the input parameters for nuclear reaction codes is necessary [8]. For these purposes, it is important to obtain more experimental measurements with high accuracy.

Numerous measured ^{59}Co(n, x) reaction cross sections are available in the EXFOR data library [9]. According to EXFOR, the ^{59}Co(n, $2n$)^{58}Co, ^{59}Co(n, p)^{59}Fe and ^{59}Co(n, α)^{56}Mn reaction cross sections are available in a wide range of neutron energies. However, the cross sections available for the ^{59}Co(n, $3n$)^{57}Co, ^{59}Co(n, $4n$)^{56}Co and ^{59}Co(n, $\alpha 2n$)^{54}Mn reactions are very much limited

Received 12 October 2020; Accepted 29 January 2021; Published online 1 March 2021

* Partly supported by the National Research Foundation of Korea (NRF) through a grant provided by the Ministry of Science and ICT (NRF-2017R1D1A1B03030484, NRF-2013M7A1A1075764, NRF-2018R1A6A1A06024970)

† E-mail: gnkim@knu.ac.kr

and scattered. Moreover, most of these data are based on the neutron energies of D+D and D+T reactions, whereas certain data are based on the neutron energy of the ^{7}Li(p, n) reaction. Thus, in this work, the ^{59}Co(n, x) reaction cross sections within the average neutron energy range of 15.2-37.2 MeV were measured by using the activation method and an off-line γ-ray spectrometric technique. We used the ^{9}Be(p, n) reaction for the production of the neutron flux. The new experimental cross section data can improve the quality of the neutron cross section database and are expected to aid in new evaluations [10]. Nuclear reaction cross sections of interest were also calculated using the computer code TALYS-1.9 [11]. The measured and calculated values from the present work were compared with the literature data provided in EXFOR and the TENDL-2019 library [12]. In this work, we focused on the analysis of the input level density, adjustable parameters for the stripping or pick-up process, and pre-equilibrium options of the TALYS-1.9 code to validate the experimental results.

II. EXPERIMENTAL DETAILS

The experiment was carried out at the MC-50 Cyclotron of the Korean Institute of Radiological and Medical Sciences (KIRAMS). A schematic view of the experimental setup is presented in Fig. 1. The fast neutrons were produced from the ^{9}Be(p, n) reaction by injecting a proton beam on a 2-mm-thick ^{9}Be metallic foil (purity ⩽ 99%) with a size of 25 mm × 25 mm. Behind the Be-target, graphite plates were used to stop the lower energy proton beam. The thickness of the graphite plates was 12 mm each for the 35 and 45 MeV proton beams and 6 mm for the 25 MeV proton beam. ^{197}Au (~0.2 gm) and ^{59}Co (~0.1 gm) foils of approximately 100 μm thickness were placed at a distance of 3.5 cm behind the Be-graphite target, as discussed in our previous work [13, 14]. The γ-ray activities for the activated sample assembly were measured using an energy-calibrated HPGe detector connected to a PC-based 4K channel analyzer. The efficiency calibration of the detector system was conducted using a standard ^{152}Eu source.

We calculated the neutron spectra using the MCNPX 2.6.0 code [15] based on the following considerations. Uwamino *et al.* [16] measured neutron spectra from the p + ^{7}Li (carbon backing) reaction with proton energies of 20, 25, 30, 35 and 40 MeV, which were simulated by Simakov *et al.* [17] using the MCNPX 2.6.0 code. The quasi-mono energetic neutron sources produced from the p+Be reaction was experimentally measured by Uwamino *et al.* [18] and estimated by Rakopoulos *et al.* [19] using the MCNPX 2.6.0 code at the Svedberg Laboratory (TSL). Novak *et al.* [20] suggested that the MCNPX 2.6.0 simulation could be used to generate the neutron spectrum for the p+Li and p+Be reactions. We calculated the neutron spectrum using the MCNPX 2.6.0 code for the Be(p, xn) reaction at a proton energy of 40 MeV and compared it with the experimental spectrum of Uwamino *et al.* [18]. The results were found to be in good agreement, except for the low neutron energy tail part. The neutron energy spectra for the p+Be reaction at proton energies of 25, 35, and 45 MeV were generated using the MCNPX 2.6.0 code and are presented in Fig. 2. The high energy distributions arose from the ^{9}Be(p, n) reaction, and the low energy tail part resulted from the break-up reaction [21]. In the present work, most of the (n, x) reactions of the ^{59}Co and ^{197}Au originated from the region of higher energy neutrons. The neutron peak energy and its width in the neutron spectra were estimated by Gaussian fitting. The FWHM of the Gaussian fitting was used to estimate the widths of the different energy peaks. The obtained peak energies and their widths were 37.20±2.20, 26.40±2.77, and 15.20±3.65 MeV for the proton beam energies of 45, 35, and 25 MeV, respectively.

III. DATA ANALYSIS

A. Neutron flux estimation

The neutron fluxes were estimated based on the

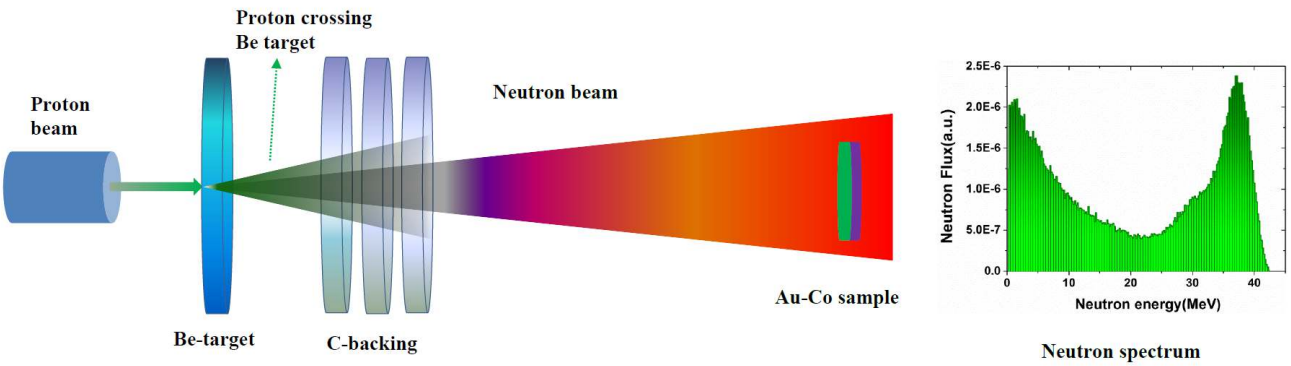

Fig. 1. (color online) Schematic view of experimental setup for irradiation facility.

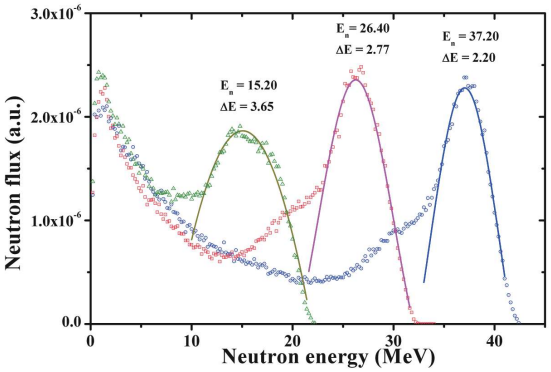

Fig. 2. (color online) Neutron spectra calculated using MCNPX 2.6.0 code for proton beam energies of 25, 35 and 45 MeV.

photo-peak activities of the 355.68 keV γ-ray of ^{196}Au from the ^{197}Au(n, 2n) reaction at 25 MeV, 98.85 keV γ-ray of ^{195}Au from the ^{197}Au(n, 3n) reaction at 35 MeV, and 293.55 keV γ-ray of ^{194}Au from the ^{197}Au(n, 4n) reaction at 45 MeV proton beams, respectively. The neutron flux $\phi_n(E_n)$ was determined from the number of observed γ-rays ($N_{\rm obs}$) under the photo-peak of an individual radionuclide of interest and the known cross sections $\sigma_R(E_n)$ of the ^{197}Au(n, xn; x=2-4) monitor reactions [22, 23]. The number of observed γ-rays ($N_{\rm obs}$) was calculated by the following formula [14]:

$$N_{\rm obs} = C \cdot \int_{E_{\rm th}}^{E_{\rm max}} \sigma_R(E_n)\phi(E_n){\rm d}E_n, \tag{1}$$

$$C = \frac{nI_\gamma\varepsilon_\gamma\left(1-{\rm e}^{-\lambda T_i}\right){\rm e}^{-\lambda T_c}\left(1-{\rm e}^{-\lambda T_{\rm clock}}\right)}{\lambda(T_{\rm clock}/T_{\rm count})}, \tag{2}$$

where n is the number of target atoms, I_γ is the branching intensity of the γ-rays of interest, ε_γ is the detection efficiency of the γ-ray, and λ is the decay constant (=ln2/$T_{1/2}$) for the produced isotope of the monitor reaction. Furthermore, $T_{\rm i}$, $T_{\rm c}$, $T_{\rm clock}$, and $T_{\rm count}$ are the irradiation time, cooling time, clock time, and counting time, respectively. The nuclear spectroscopic data of the investigated radionuclides were obtained from the Lund University and Lawrence Berkeley National Laboratory database [24], which are presented in Table 1.

The neutron fluxes were determined in the neutron energy region from the reaction threshold of the ^{197}Au(n, xn; x=2-4) monitor reactions to the maximum neutron energies. The $N_{\rm obs}$ values under the characteristic photo-peak of the γ-rays of the reaction products $^{194\text{-}196}$Au were related to the neutron flux $\phi_n(E_n)$ and cross sections $\sigma_R(E_n)$ of the ^{197}Au(n, xn; x=2-4) monitor reactions, which were obtained from the TENDL-2019 [14] library. However, the measured neutron flux for the peak neutron energy region $\phi_n(E_n)$ from $E_P-\Delta E$ to $E_P+\Delta E$ was estimated using the modified number of γ-rays $M_{\rm obs} = C_{br}\cdot N_{\rm obs}$. The correction factor C_{br} can be calculated as the ratio of $M_{\rm obs}$ to $N_{\rm obs}$ [2, 25, 26]:

$$C_{br} = \frac{M_{\rm obs}}{N_{\rm obs}} = \frac{\int_{E_P-\Delta E}^{E_P+\Delta E}\sigma_R(E_n)\phi_n(E_n){\rm d}E_n}{\int_{E_{th}}^{E_{\rm max}}\sigma_R(E_n)\phi_n(E_n){\rm d}E_n}, \tag{3}$$

where $\phi_n(E_n)$ is the neutron flux calculated using the MCNPX 2.6.0 code, as shown in Fig. 2, $E_{\rm th}$ and $E_{\rm max}$ are the reaction thresholds of the monitor reactions and maximum neutron energy according to the proton energy, E_p is the peak neutron energy, and ΔE is the standard devi-

Table 1. Nuclear spectroscopic data of radio-nuclides from ^{59}Co(n, x) and ^{197}Au(n, xn) reactions and calculated factors (C_{br}).

S. No	Nuclide	Jπ	$T_{1/2}$	Decay mode	E_γ/keV	I_γ(100)	Contributing reaction	$E_{\rm th}$/MeV	C_{br} (Calculated)		
									25 MeV	35 MeV	45 MeV
					Reactions studied						
1.	^{58}Co	2^+	70.86 d	EC	810.78	99.00	^{59}Co(n, 2n)	10.63	0.87	0.36	0.20
2.	^{57}Co	$7/2^-$	271.79 d	EC	122.06 136.47	85.60 10.68	^{59}Co(n, 3n)	19.35	–	0.79	0.39
3.	^{56}Co	4^+	77.27 d	EC	846.77 1238.28	100.0 67.6	^{59}Co(n, 4n)	31.00	–	–	0.73
4.	^{59}Fe	$3/2^-$	44.50 d	β^-	1099.25 1291.60	56.5 43.2	^{59}Co(n, p)	0.800	0.56	0.28	0.14
5.	^{56}Mn	3^+	2.58 h	β^-	846.77	98.9	^{59}Co(n, α)	3.800	0.74	0.24	0.18
6.	^{54}Mn	3^+	312.3 d	EC	834.85	99.98	^{59}Co(n, α2n)	12.14	–	0.61	0.59
					Monitor reactions						
7.	^{196}Au	2^-	6.18 d	EC(93); β^-(7)	355.68	87.00	^{197}Au(n, 2n)	8.11	087	–	–
8.	^{195}Au	$3/2^+$	186.09 d	EC	98.85	10.90	^{197}Au(n, 3n)	14.79	–	0.67	–
9.	^{194}Au	1^-	38.02 h	EC	293.55	10.4	^{197}Au(n, 4n)	23.21	–	–	0.58

ation of the Gaussian fitted neutron spectra presented in Fig. 2. The calculated correction factors C_{br} were obtained and are presented in Table 1. The cross section $\bar{\sigma}_{RP}$ could be assumed as constant over the peak width. Subsequently, the neutron fluence at the peak neutron energy ϕ_{nP} was obtained by means of Eq. (4):

$$\phi_{nP} = \int_{E_p-\Delta E}^{E_p+\Delta E} \phi_n(E_n)\,\mathrm{d}E_n \approx \frac{C_{br}\cdot N_{\rm obs}}{\bar{\sigma}_{RP}}. \tag{4}$$

B. Reaction cross section calculation

The C_{br} parameters were also estimated for the ^{59}Co(n, x) reactions using the cross sections from the TENDL-2019 library and the calculated neutron spectra in Fig. 2. In this case, only the relative values of the cross sections were meaningful, as indicated in Eq. (4). The estimated C_{br} parameters are listed in Table 1. Thereafter, the absolute production cross-sections ($\bar{\sigma}_{RP}$) for the radio-nuclides ^{56}Mn, ^{54}Mn, ^{59}Fe, ^{58}Co, ^{57}Co, and ^{56}Co at the peak neutron energies were obtained according to the following formula:

$$\bar{\sigma}_{RP} = \frac{C_{br}}{C}\cdot\frac{N_{\rm obs}}{\phi_{nP}}. \tag{5}$$

IV. RESULTS AND DISCUSSION

The measured cross sections for the ^{59}Co(n, x)$^{56\text{-}58}$Co, ^{59}Co(n, p)^{59}Fe, and ^{59}Co(n, αxn)^{54,56}Mn reactions based on Eq. (5) are presented in Table 2. The uncertainties of the measured cross sections were obtained, which were between 10.0% and 16.7%. The overall uncertainty was the quadratic sum of both the statistical and systematic errors. The statistical error resulted from counting statistics and was estimated to be 1.0%-4.0%. The systematic errors were owing to uncertainties in the irradiation time (~0.5%), the detection efficiency calibration (~4%), the uncertainty in the neutron flux (7.4%-14.8%), the half-life of the nuclides of interest, and the γ-ray abundance (~2%). The uncertainty in the neutron flux arose from the uncertainty in the cross section for the monitor reaction, the uncertainty owing to the subtraction of the low energy tail in the neutron spectrum, and the statistical uncertainty of the observed photo-peak count of the γ-ray from the reaction product of the monitor reaction. Honusek *et al.* [26] proposed an error of 5% in the neutron flux resulting from the subtraction of the low-energy tail in the neutron spectrum based on the MCNPX 2.6.0 simulation. The uncertainties in the cross sections of the monitor reactions were 7.568% for the ^{197}Au(n, 2n), 5.0% for the ^{197}Au(n, 3n), and 13.0% for the ^{197}Au(n, 4n) monitor reactions. The statistical uncertainty of the observed photo-peak count for the γ-ray from the reaction product of the monitor reaction was only 2.2%-1.9%. Thus, based on the quadratic sum of the values from the three sources, the uncertainty in the neutron flux was 7.4%-14.8%. The uncertainties in the nuclear reaction cross sections (σ_x) of the present work were also obtained based on the quadratic sum formula, which is given as

$$\left(\frac{\Delta\sigma_x}{\sigma_x}\right)^2 = \sum_q \left(\frac{\Delta q_x}{q_x}\right)^2, \tag{6}$$

where the parameters $\left(q = N_{\rm obs}, T_i, I_\gamma, \varepsilon_\gamma, C_{br}, \phi_{nP}\right)$ that appear on the right-hand side of Eq. (6) are independent.

The results obtained in this work, together with the literature data, are shown in Figs. 3-8. The theoretical results were obtained from the TALYS-1.9 code with default and adjusted parameters for each investigated radionuclide. In the theoretical calculation using the TALYS-1.9 code with the back-shifted Fermi gas model, the three input parameters *ldmodel*, *Cstrip a* (0.7), *alphald* (0.102), and *betald* (0.11) played a vital role. Thus, these three parameters were adjusted within their recommended limits to obtain the excitation functions with relatively good descriptions of the experimental data. We compared the measured cross sections with the theoretical values obtained from the TALYS-1.9 code and data from the TENDL 2019 library.

A. ^{59}Co(n, 2n)^{58}Co reaction

The long-lived radionuclide ^{58}Co ($T_{1/2}$=70.86 d) was produced from the ^{59}Co(n, 2n)^{58}Co reaction with a threshold energy of 10.63 MeV, which decayed to ^{58}Fe with the EC (100%) process. The ^{58}Co was identified by the intense γ-line of 810.77 keV (I_γ = 99%). The cross sections of the ^{59}Co(n, 2n)^{58}Co reaction at neutron energies of 15.20±3.65, 26.40±2.77, and 37.20±2.20 MeV were obtained and are presented in Table 2. The measured cross sections of the present work, along with the literature data [2, 27-37], data from the TENDL 2019 library [12], and the theoretical values obtained using TALYS-1.9 with default parameters (TALYS-1.9 (default)) and TALYS-1.9 with adjusted parameters (TALYS-1.9 (adjusted)) are shown in Fig. 3. The theoretical values obtained from TALYS-1.9 (default) were in good agreement with the experimental values up-to 20 MeV but were underestimated at higher neutron energies. However, the theoretical values from TALYS-1.9 (adjusted) agreed well with the present data. A comparison of the present data with the literature data [20-31] and theoretical values demonstrated good agreement at neutron energies of 26.40±2.77 and 37.20±2.20 MeV, which confirmed the reliability of the present technique. However, the present results at a neutron energy of 15.20±3.65 MeV was slightly lower than the literature data and theoretical values. This may be owing to the broad neutron spectrum for the proton energy of 25 MeV.

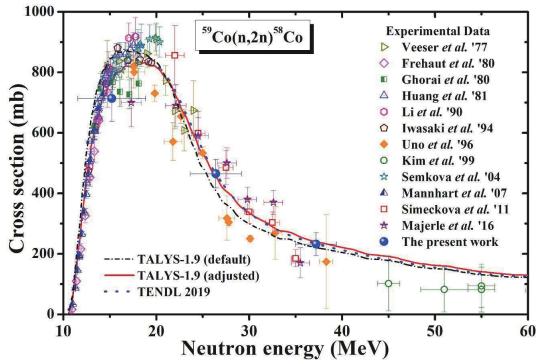

Fig. 3. (color online) Comparison of ^{59}Co(n, $2n$)^{58}Co reaction cross sections from present work with literature data and theoretical values. In this figure, TALYS-1.9 (default) and TALYS-1.9 (adjusted) indicate the theoretical data obtained using the TALYS-1.9 code with default and adjusted parameters, respectively.

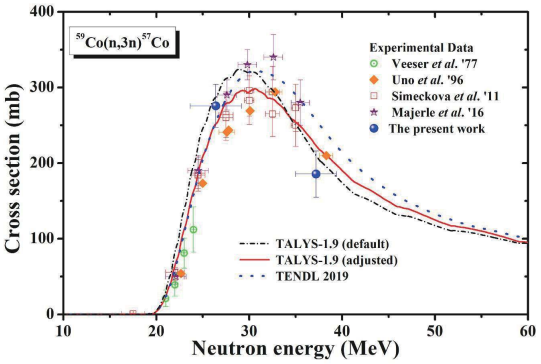

Fig. 4. (color online) Comparison of ^{59}Co(n, $3n$)^{57}Co reaction cross sections from present work with literature data and theoretical values. In this figure, TALYS-1.9 (default) and TALYS-1.9 (adjusted) indicate the theoretical data obtained using the TALYS-1.9 code with default and adjusted parameters, respectively.

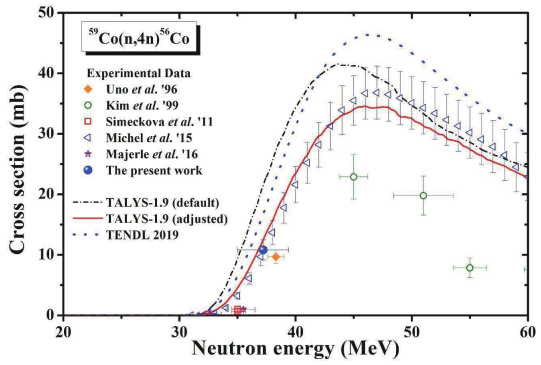

Fig. 5. (color online) Comparison of ^{59}Co(n, $4n$)^{56}Co reaction cross sections from present work with literature data and theoretical values. In this figure, TALYS-1.9 (default) and TALYS-1.9 (adjusted) indicate the theoretical data obtained using the TALYS-1.9 code with default and adjusted parameters, respectively.

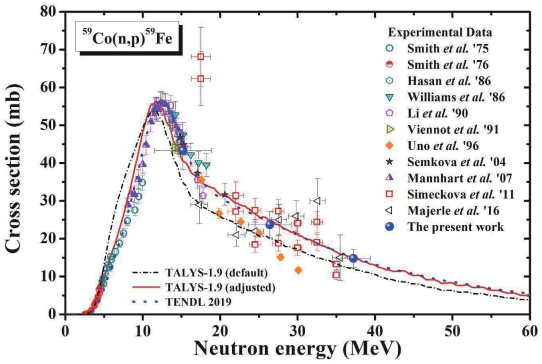

Fig. 6. (color online) Comparison of ^{59}Co(n, p)^{59}Fe reaction cross sections from present work with literature data and theoretical values. In this figure, TALYS-1.9 (default) and TALYS-1.9 (adjusted) indicate the theoretical data obtained using the TALYS-1.9 code with default and adjusted parameters, respectively.

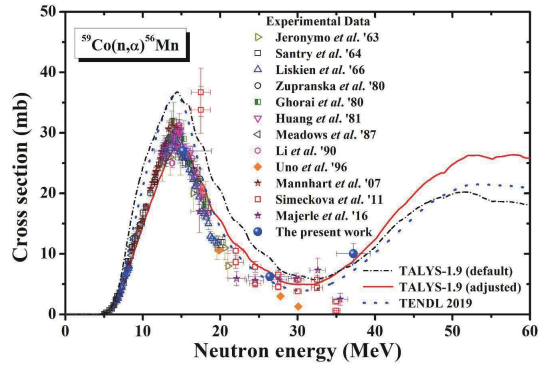

Fig. 7. (color online) Comparison of ^{59}Co(n, α)^{56}Mn reaction cross sections from present work with literature data and theoretical values. In this figure, TALYS-1.9 (default) and TALYS-1.9 (adjusted) indicate the theoretical data obtained using the TALYS-1.9 code with default and adjusted parameters, respectively.

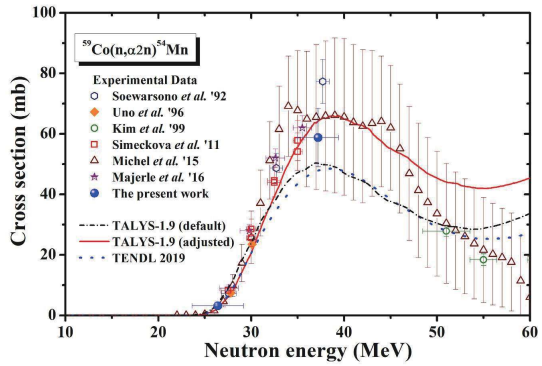

Fig. 8. (color online) Comparison of ^{59}Co(n, α$2n$)^{54}Mn reaction cross sections from present work with literature data and theoretical values. In this figure, TALYS-1.9 (default) and TALYS-1.9 (adjusted) indicate the theoretical data obtained using the TALYS-1.9 code with default and adjusted parameters, respectively.

Table 2. Measured cross sections of the ^{59}Co(n, x) reactions.

E_n/MeV	Reaction cross section/mb					
	^{59}Co(n, 2n)^{58}Co	^{59}Co(n, 3n)^{57}Co	^{59}Co(n, 4n)^{56}Co	^{59}Co(n, p)^{59}Fe	^{59}Co(n, α)^{56}Mn	^{59}Co(n, α2n)^{54}Mn
15.20±3.65	712.42±74.81	–	–	43.31±4.95	27.02±2.82	–
26.40±2.77	464.60±47.19	275.65±28.48	–	23.69±3.47	6.25±0.69	3.18±0.43
37.20±2.20	232.11±38.06	185.48±31.75	10.815±1.89	14.81±2.43	10.04±1.71	58.74±9.67

B. ^{59}Co(n, 3n)^{57}Co reaction

The long-lived radionuclide ^{57}Co ($T_{1/2}$= 271.79 d) was produced from the ^{59}Co(n, 3n)^{57}Co reaction with a threshold energy of 19.35 MeV, which decayed to ^{57}Fe with the EC (100%) process. The cross section of the ^{59}Co(n,3n)^{57}Co reaction was measured by the intense γ-lines of 122.06 keV (I_γ = 85.6%) and 136.47 keV (I_γ = 10.68%). We counted two γ-lines with a long counting time to reduce the statistical uncertainties. We obtained the cross sections of the ^{59}Co(n, 3n)^{57}Co reaction at neutron energies of 26.40±2.77 and 37.20±2.20 MeV, and these values are listed in Table 2. The measured reaction cross sections of the present work, along with the literature data, TENDL-2019 data, and theoretical values obtained from TALYS-1.9 with default and adjusted parameters are presented in Fig. 4. It can be observed from Fig. 4 that the theoretical values from the TALYS-1.9 code with default parameters were overestimated compared to the experimental data below 35 MeV, whereas the data from the TENDL 2019 library were overestimated above 30 MeV. In the theoretical calculation, the two input parameters "*Pshiftadjust*" and "*s2adjust*" drastically changed the curve. The measured value at a neutron energy of 26.40±2.77 MeV was found to be in good agreement with the literature data [2, 27, 33, 37] and the theoretical values. However, the present value at the neutron energy of 37.20±2.20 MeV was slightly lower than the theoretical value.

C. ^{59}Co(n, 4n)^{56}Co reaction

The long-lived radionuclide ^{56}Co ($T_{1/2}$ = 77.27 d) was produced from the ^{59}Co(n, 4n)^{56}Co reaction with a threshold energy of 31.0 MeV, which decayed to ^{56}Fe with the EC (100%) process. The radionuclide ^{56}Co was identified via the 846.77 keV (I_γ = 100%) and 1238.28 keV (I_γ = 67.6%) γ-rays. In the present work, the ^{59}Co(n, 4n)^{56}Co reaction cross section was obtained at a neutron energy of 37.20±2.20 MeV and is displayed in Table 2. The measured reaction cross section, along with the literature data [2, 33, 34, 37, 38], TENDL 2019 data, and theoretical values from TALYS-1.9 with default and adjusted parameters are shown in Fig. 5. It can be observed from Fig. 5 that the theoretical data from the TALYS-1.9 (default) and TENDL 2019 data were overestimated compared to the experimental values. The theoretical value of the TALYS-1.9 (adjusted) was described better when estimate the cross section at low and higher neutron energies. The values reported by Kim *et al*. [34] were drastically underestimated in the other experimental values and the theoretical data. The theoretical data using the TALYS-1.9 code reproduced the present results very well.

D. ^{59}Co(n, p)^{59}Fe reaction

The radionuclide ^{59}Fe was produced from the ^{59}Co(n, p)^{59}Fe reaction at neutron energies of 15.20±3.65, 26.40±2.77, and 37.20±2.20 MeV. The threshold energy for the ^{59}Co(n, p)^{59}Fe reaction was 0.8 MeV. The reaction product ^{59}Fe ($T_{1/2}$ = 44.5 d) decayed to ^{59}Co through the β^- decay (100%). It was identified by the intense γ-lines of 1099.25 keV (I_γ = 56.5.0%) and 1291.6 keV (I_γ = 43.2%). We obtained data with different cooling times and finally determined their average values. The cross sections for the ^{59}Co(n, p)^{59}Fe reaction from the present work are presented in Table 2. The present results were compared with the literature data [2, 31, 33, 35-37, 39-43], TENDL 2019 data, and calculated values from the TALYS-1.9 code, as illustrated in Fig. 6. The theoretical values from TALYS-1.9 (default) were overestimated below 10 MeV and underestimated above 10 MeV compared to the experimental data. The theoretical values from TALYS-1.9 (adjusted) and the TENDL 2019 data were consistent with the present data. The pre-equilibrium process started after the sharp peak of the compound nucleus. In particular, the "*Pshiftadjust*" parameter was used to obtain a relatively good description of the experimental data at the pre-equilibrium process. The theoretical results obtained from TALYS-1.9 with adjusted parameters at lower and higher energies were described better than those with default parameters. The present data agreed very well with the theoretical values obtained from TALYS-1.9 with adjusted parameters over the investigated energy range.

E. ^{59}Co(n, α)^{56}Mn reaction

The radionuclide ^{56}Mn was produced from the ^{59}(n, α)^{56}Mn reaction with a threshold energy of 3.80 MeV. The radionuclide ^{56}Mn ($T_{1/2}$ = 2.58 h) underwent 100% β^- decays to produce ^{56}Fe. It was identified by an intense γ-line of 846.77 keV (I_γ = 98.9%). We measured the cross sections of the ^{59}(n, α)^{56}Mn reaction at neutron energies of 15.20±3.65, 26.40±2.77, and 37.20±2.20 MeV, as lis-

ted in Table 2. The present data were compared with the literature data [2, 29-31, 33, 36, 37, 44-48], data from the TENDL 2019 library, and theoretical values from TALYS-1.9 with default and adjusted parameters, as shown in Fig. 7. Fig. 7 indicates that the theoretical data from the TALYS-1.9 code with default parameters were overestimated compared to the experimental values. The theoretical calculations using the TALYS-1.9 code with adjusted parameters, such as the "*Pshiftadjust*" and "*s2adjust*" parameters, were used to obtain a relatively good description of the experimental data at the pre-equilibrium process. We obtained good agreement among the different experimental values. The calculated values using TALYS-1.9 with adjusted parameters at lower and higher neutron energies described the experimental data better than those with default parameters. Relatively good agreement was obtained between the present data and the theoretical data obtained from TALYS-1.9 with adjusted parameters in the investigated energy range.

F. ^{59}Co(n, α2n)^{54}Mn reaction

The relatively long-lived radionuclide ^{54}Mn was produced through the ^{59}Co(n, α2n) (E_{th} =12.14 MeV) reaction with neutron energies of 26.40±2.77 and 37.20±2.20 MeV. The reaction product ^{54}Mn ($T_{1/2}$ =312.3 d) decayed to ^{54}Cr through the EC (100%) process and it was identified by an intense γ-line of 834.85 keV (I_γ = 99.98%). The γ-ray spectrometry was performed with a long counting time to guarantee good counting statistics. We obtained data with different cooling times and finally determined their average values, as listed in Table 2. We compared the present data with the literature data [2, 33, 34, 37, 38, 49], as shown in Fig. 8. The theoretical data from the TALYS-1.9 code with default parameters and the data from the TENDL 2019 library were underestimated compared to the experimental values around the 40 MeV region, which was possibly owing to the underestimation of the compound nucleus processes. The experimental cross sections up to 30 MeV were in good agreement with the values from the TALYS-1.9 calculation using default and adjusted parameters. However, the calculated cross sections for the ^{59}Co(n, α2n)^{54}Mn reaction based on TALYS-1.9 with adjusted parameters were in good agreement with the experimental values. It can be observed from Fig. 8 that the theoretical data from the TALYS-1.9 code with adjusted parameters were consistent with the experimental data up to 45 MeV.

V. CONCLUSION

We measured new cross sections for the ^{59}Co(n, x) reactions in the neutron energy range between 15.2 and 37.2 MeV based on the ^{9}Be(p, xn) reaction. The present data were compared with the literature data, TENDL 2019 data, and the theoretically calculated values using TALYS-1.9. Most of the present data were in good agreement with the existing literature data. The experimentally measured ^{59}Co(n, x) reaction cross sections from the present work and literature were comparable with the theoretical values from TALYS-1.9 with adjusted parameters. Thus, the experimental results of the present work will be useful as a benchmark to evaluate nuclear data. The results can also aid in determining the appropriate parameters for statistical models to obtain accurate neutron induced reaction cross sections of ^{59}Co.

ACKNOWLEDGEMENTS

The authors are thankful to the staff of the MC50 Cyclotron Laboratory at the Korea Institute of Radiological and Medical Sciences (KIRAMS) for the excellent operation and their support during the experiment.

References

[1] N. Dzysiuk, I. Kadenko, A. Koning *et al*., Phys. Rev. C **81**, 014610 (2010)
[2] E. Simeckova, P. Bem, V. Burjan *et al*., J. Kor. Nucl. Soc. **59**, 1801 (2011)
[3] S. Spellerberg, P. Reimer, G. Blessing *et al*., Appl. Radiat. Isot. **49**, 1519 (1998)
[4] M. U. Khandaker, H. Haba, J. Kanaya *et al*., Nucl. Instrum. Methods Phys. Res. B **316**, 33 (2013)
[5] R. Baldık and A. Yılmaz, Nuclear Science and Techniques **29**, 156 (2018)
[6] M. Chadwick, P. Obložinský, M. Herman *et al*., Nuclear data sheets **107**, 2931 (2006)
[7] A. V. Voinov, S. M. Grimes, C. R. Brune *et al*., Phys. Rev. C **88**, 054607 (2013)
[8] M. Herman, R. Capote, B. Carlson *et al*., Nuclear data sheets **108**, 2655 (2007)
[9] Cross Section Information Storage and Retrieval System (EXFOR), Vienna, Austria, http://www.nds.iaea.or.at/exfor/(online)
[10] X.-J. Sun, F.-Q. Zhou, Y.-L. Song *et al*., Chinese Physics Letters **36**, 112501 (2019)
[11] A. J. Koning and D. Rochman, Nuclear Data Sheets **113**, 2841 (2012)
[12] A. J. Koning, D. Rochman, J. Sublet *et al*., Nuclear Data Sheets 155: 1 (2019), available from: https//tendl.web.psi.ch/tendl_2019/tendl2019.html
[13] M. Zaman, G. N. Kim, K. Kim *et al*., Eur. Phys. J. A **51**, 104 (2015)
[14] M. Zaman, G. N. Kim, K. Kim *et al*., Eur. Phys. J. A **53**, 182 (2017)
[15] J. S. Hendricks, W. M. Gregg, L. F. Michael *et al.*, MCNPX 2.6.0 Extensions, LANL Report LA-UR-08-2216, Los Alamos, URL http://mcnpx.lanl.gov/, (2008)
[16] Y. Uwamino, T. S. Soewarsono, H. Sugita *et al*., Nucl. Instrum. Methods Phys. Res. A **389**, 463 (1997)
[17] S. Simakov, P. Bém, V. Burjan *et al*., J. Kor. Nucl. Soc. **59**,

1856 (2011)
[18] Y. Uwamino, T.-o. Ohkubo, A. Torii *et al.*, Nucl. Instrum. Methods Phys. Res. A **271**, 546 (1988)
[19] V. Rakopoulos, M. Lantz, P. Andersson *et al.*, EPJ Web of Conferences **66**, 11032 (2014)
[20] J. Novák, P. Bém, U. Fischer *et al.*, in *EPJ Web of Conferences* (EDP Sciences, 2010), p. 06001
[21] H. Yashima, S. Sekimoto, T. Utsunomiya *et al.*, Proc. Radioch. A Suppl. Radio. Acta **1**, 135 (2011)
[22] B. P. Bayhurst, J. S. Gilmore, R. J. Prestwood *et al.*, Phys. Rev. C **12**, 451 (1975)
[23] Y. Uwamino, H. Sugita, Y. Kondo *et al.*, Nucl. Data Sci. Tech., 726 (1992)
[24] S. Y. F. Chu, L. F. Ekstrom, and R. B. Firestone, Lund/LBNL Nuclear Data Service, Version 2.0, http://nucleardata.nuclear.lu.se/nucleardata/toi/
[25] P. Chudoba, S. Kilim, V. Wagner *et al.*, Phys. Proc. **59**, 114 (2014)
[26] M. Honusek, P. Bém, U. Fischer *et al.*, J. Kor. Phys. Soc. **59**, 1374 (2011)
[27] L. R. Veeser, E. D. Arthur, and P. G. Young, Phys. Rev. C **16**, 1792 (1977)
[28] J. Frehaut, A. Bertin, R. Bois *et al.*, Proc. of Symposium on Neutron Cross Sections from 10 to 50 MeV, Brookhaven National Laboratory Upton, New York 11973, May 12-14, (1980)
[29] S. Ghorai, J. Gaiser, and W. Alford, Annals of Nuclear Energy **7**, 41 (1980)
[30] J. Huang, H. Lu, J. Li *et al.*, Chinese J. of Nuclear Physics (Beijing) **3**, 59 (1981)
[31] T. Li, High Energy Phys. Nucl. Phys.,.. Chinese Ed. **14**, 542 (1990)
[32] S. Iwasaki, S. Matsuyama, T. Ohkubo *et al.*, in *Proc. of Int. Conf. on Nucl. Data Sci. Tech., ed. JK Dickens, Gatlinburg, Tennessee*, May1994), pp. 9
[33] Y. Uno, S. Meigo, S. Chiba *et al.*, in *9th International Symposium on Reactor Dosimetry, September 2-6, 1996, Prague, Czech Republic*1996), pp. 465
[34] E. J. Kim, T. Nakamura, Y. Uwamino *et al.*, Journal of Nuclear Science and Technology **36**, 29 (1999)
[35] V. Semkova, V. Avrigeanu, T. Glodariu *et al.*, Nucl. Phys. A **730**, 255 (2004)
[36] W. Mannhart and D. Schmidt, Physikalisch Technische Bundesanstalt, Braunschweig (Germany). Neutronenphysik, PTB N 54 (2007)
[37] M. Majerle, P. Bém, J. Novák, *et al.*, Nucl. Phys. A **953**, 139 (2016)
[38] R. Michel, D. Hansmann, S. Neumann, *et al.*, Nucl. Instrum. Methods Phys. Res. B **343**, 30 (2015)
[39] D. L. Smith and J. W. Meadows, Nucl. Sci. Eng. **58**, 314 (1975)
[40] D. L. Smith and J. W. Meadows, Nucl. Sci. Eng. **60**, 187 (1976)
[41] S. Hasan, A. Pavlik, G. Winkler *et al.*, Journal of Physics G: Nuclear Physics **12**, 397 (1986)
[42] J. Williams, W. Alford, and S. Ghorai, Radiation Effects **92**, 215 (1986)
[43] M. Viennot, M. Berrada, G. Paic *et al.*, Nucl. Sci. Eng. **108**, 289 (1991)
[44] J. Jeronymo, G. Mani, J. Olkowsky *et al.*, Nuclear Physics **47**, 157 (1963)
[45] D. Santry and J. Butler, Canadian J. of Phys. **42**, 1030 (1964)
[46] H. Liskien and A. Paulsen, Journal of Nuclear Energy. Parts A/B. Reactor Science and Technology **19**, 73 (1965)
[47] E. Zupranska, K. Rusek, J. Turkiewicz *et al.*, Acta Physica Polonica. Series B **11**, 853 (1980)
[48] J. Meadows, D. Smith, M. Bretscher *et al.*, Annals of Nuclear Energy **14**, 489 (1987)
[49] T. S. Soewarsono, Y. Uwamino, and T. Nakamura, Nucl. Instrum. Meth. A **389**, 463 (1997)